PNAS
www.pnas.org

Supplementary Information for

Structure of an amorphous calcium carbonate phase involved in the formation of *Pinctada margaritifera* shells

Tilman A. Grünewald, Stefano Checcia, Hamadou Dicko, Gilles Le Moullac, Manaarii Sham Koua, Jeremie Vidal-Dupiol, Julien Duboisset, Julius Nouet, Olivier Grauby, Marco Di Michiel and Virginie Chamard

Corresponding author: Tilman A. Grünewald
Email: tilman.grunewald@fresnel.fr

This PDF file includes:

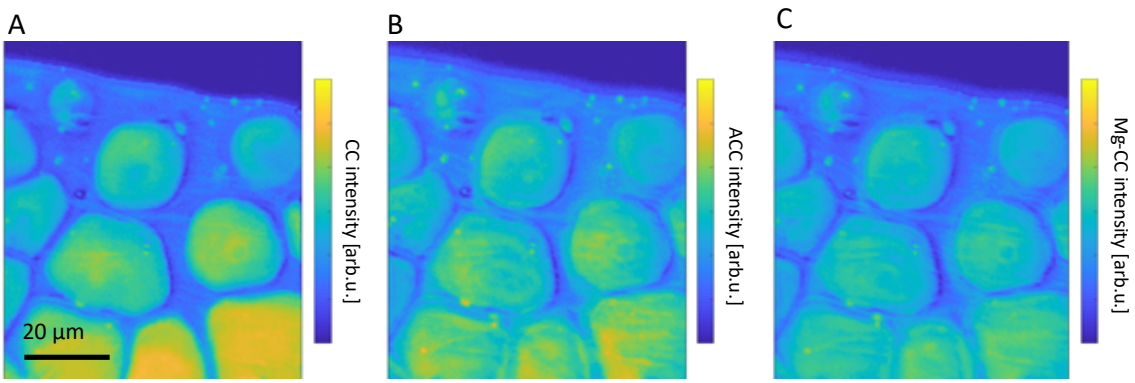

Fig. S1. SRS intensity maps. (A) SRS intensity map at the crystalline calcite (CC) wavenumber (1084 – 1086 cm^{-1}). (B) SRS intensity map at the amorphous calcium carbonate (ACC) wavenumber (1073 – 1081 cm^{-1}). (C) SRS intensity map at the Mg-calcite (Mg-CC) wavenumber (1092 – 1093 cm^{-1}). Note that all maps are scaled to the same intensity level.

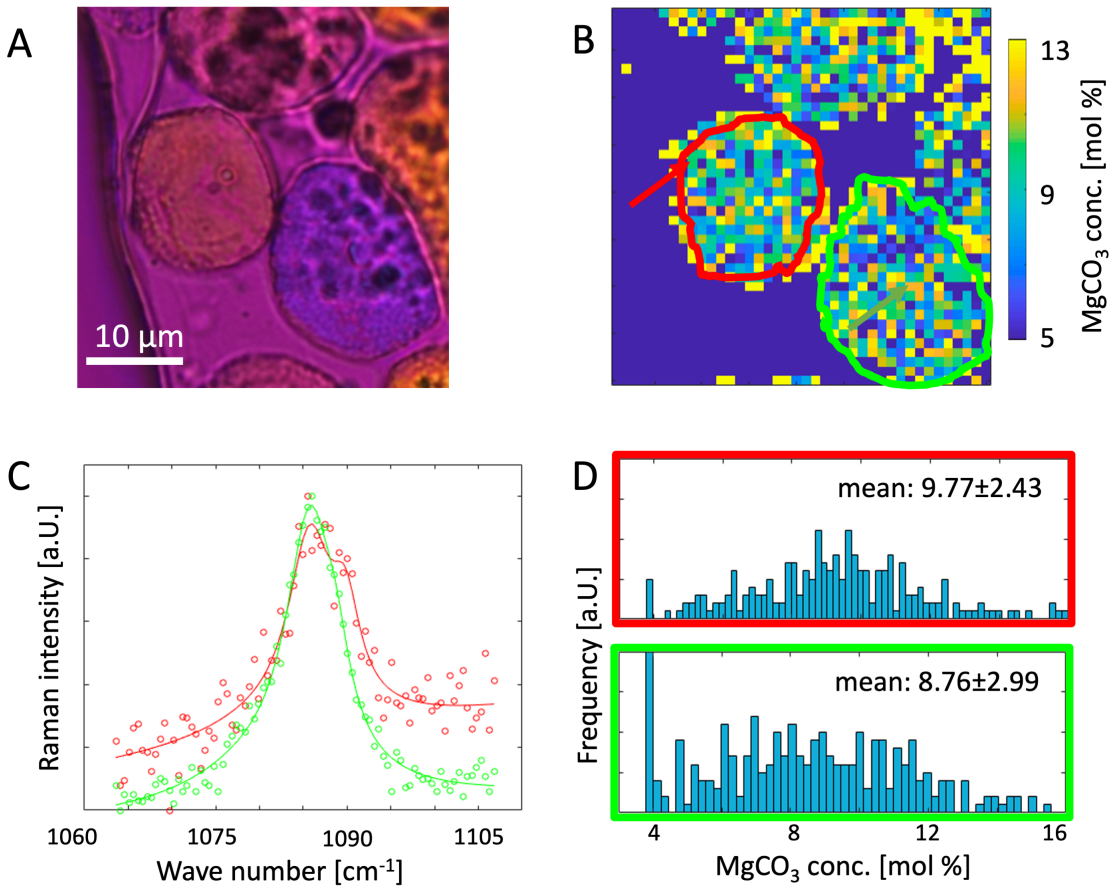

Fig. S2. Micro-Raman spectroscopy. (A) Polarized light microscope image of the sample area, with growth edge on the left-hand side. (B) $MgCO_3$ concentration in the Mg-calcite crystal extracted from the v1 peak position. (C) Two spectra (open symbols) and the corresponding peak fits (solid lines) for a spot at the margins of a disc (red curve, red arrow in (B)) and a mature prism (green curve, green arrow in (B)). The additional shoulder at higher wavenumbers is indicative of the presence of the Mg-CC phase content. (D) Histograms of the $MgCO_3$ content for a young disc (red outline in (B)) and mature prism (green outline in (B)), showing a higher $MgCO_3$ content for the young prism. The mean and standard deviation are reported in the histograms and the t-test results indicate significant difference (p=0.009). The full fit results are reported in Fig S3.

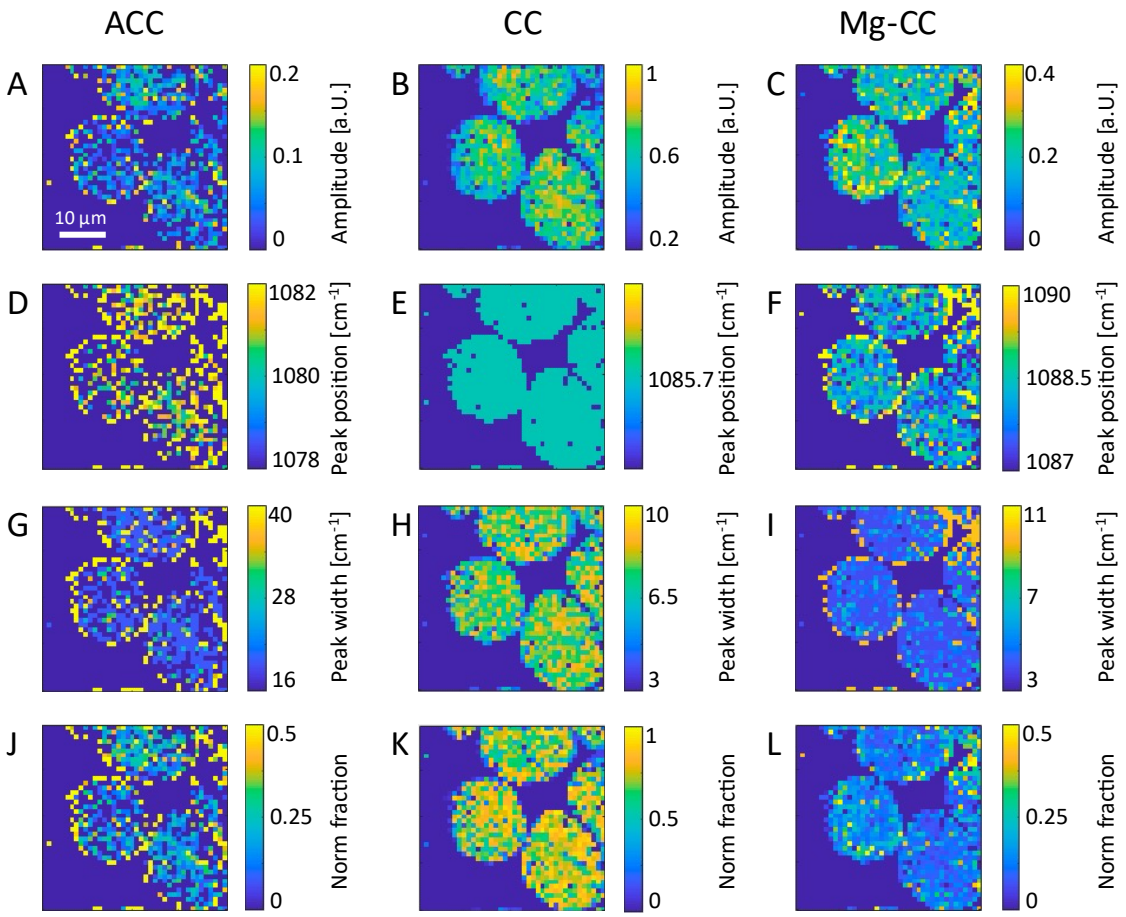

Fig. S3. Peak deconvolution of the micro-Raman spectroscopy (A-C) Peak amplitude of the ACC, CC and Mg-CC peak contribution respectively (D-F) Peak position of the ACC, CC and Mg-CC peaks respectively. Note that the CC peak position was fixed to accurately determine the ACC and Mg-CC contribution. (G-I) Peak width of the ACC, CC and Mg-CC contribution respectively. (J-L) Normalised fraction (normalized peak area) of the ACC, CC and Mg-CC contribution.

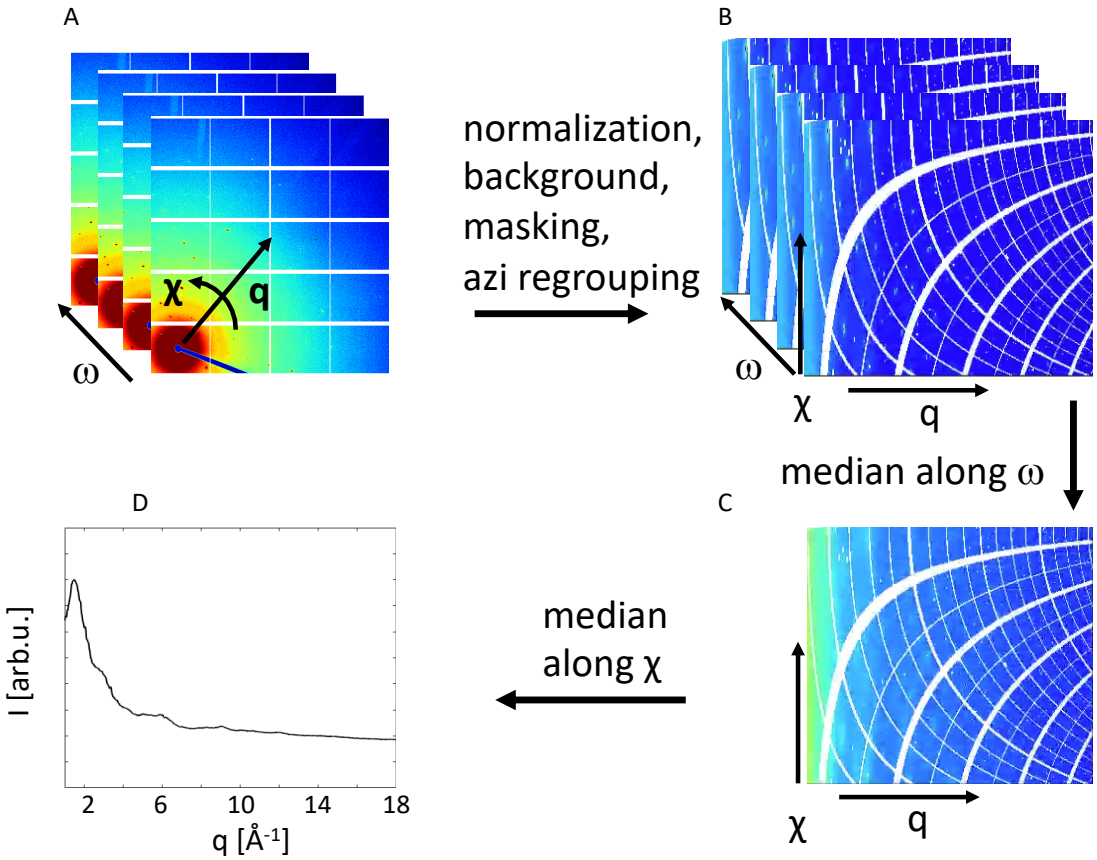

Fig. S4. Data processing steps for PDF measurements. (A) The raw data comprised a series of diffraction patterns recorded at different ω rotation angles. (B) The data is processed by intensity normalization, background subtraction, masking of defective pixels and converted by azimuthal regrouping. (C) The image stack is median filtered along ω and χ to isolate the diffuse scattering component from diffracted reflections. (D) The resulting scattering curve of the PDF data.

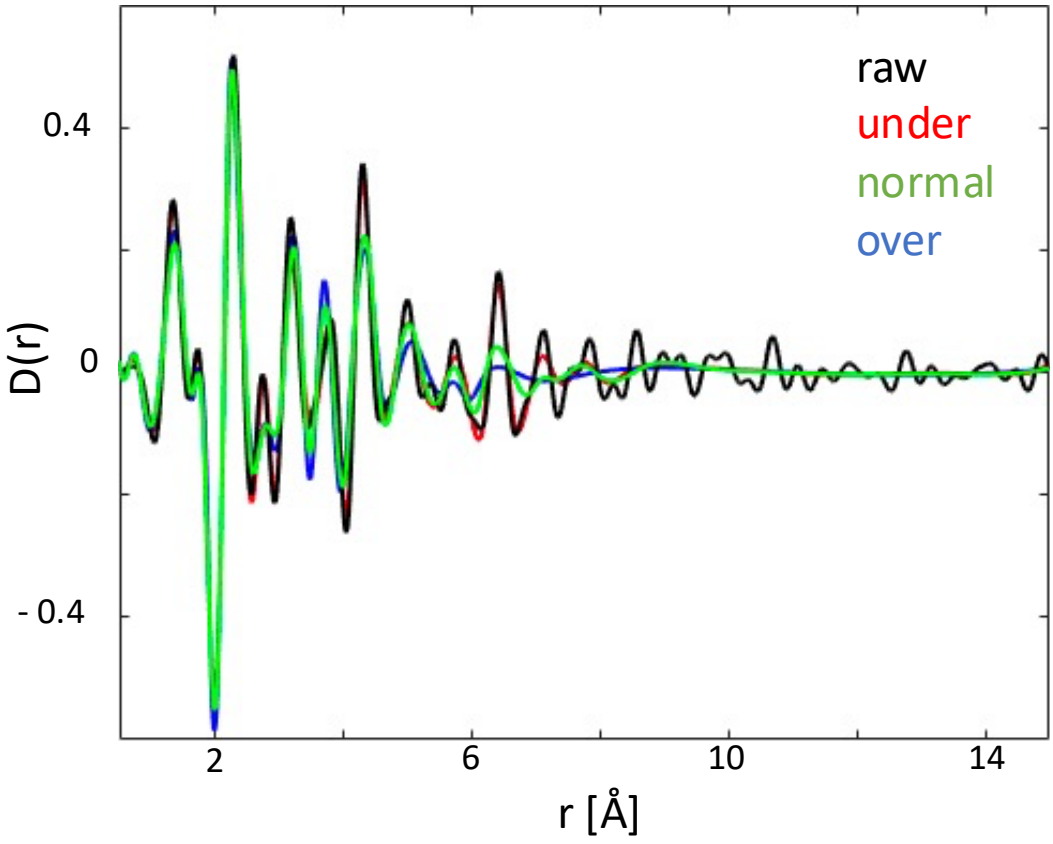

Fig. S5. Comparison of spline smoothing procedure to reduce the spurious effects of intensity outliers. Raw signal (black) compared to a weak spline (red), the normal, chosen (green) spline strength and the strong spline (blue)

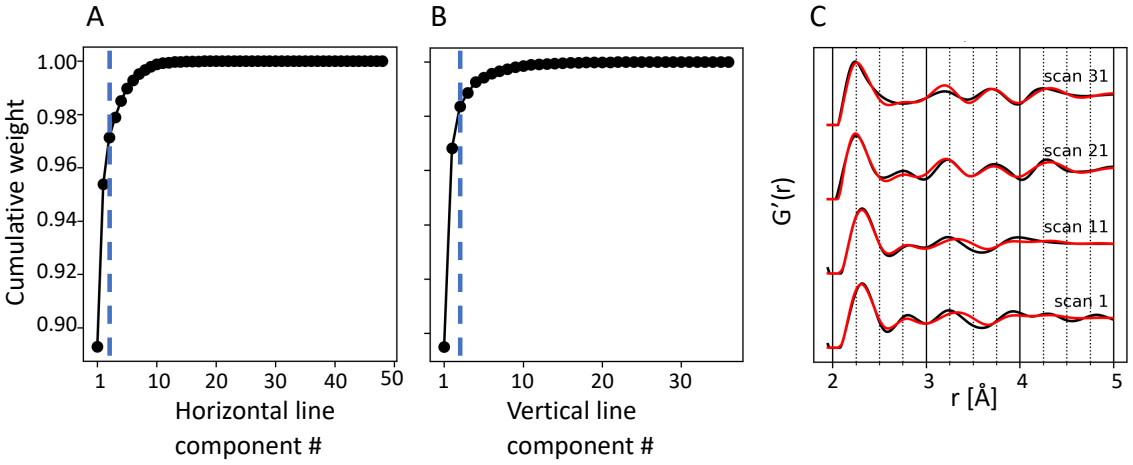

Fig. S6. PCA analysis (A) Cumulative weight of the extracted PCs for the horizontal line, blue line indicates the chosen threshold for 3 PCs (B) Cumulative weight of the extracted PCs for the vertical line, blue line indicates the chosen threshold for 3 PCs (C)

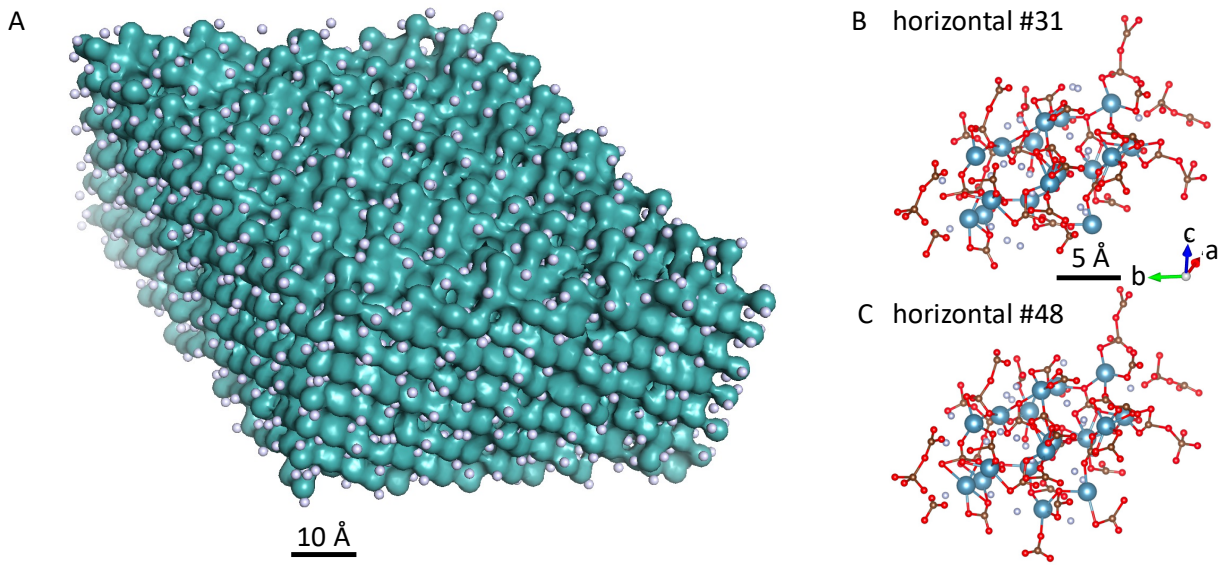

Fig. S7. Atomic configuration obtained from the RMC modelling. (A) The full super cell (horizontal line #31) with the $CaCO_3$ shown as a turquoise isosurface and the water oxygen atoms shown as grey spheres. (B) Detail from the center of the model (horizontal #31, young prism position). The Ca, C and O atoms of the $CaCO_3$ are shown as blue, brown and red spheres and the water oxygen as grey spheres. (C) Detail from the center of the model (horizontal #48, mature prism position). The position of the Ca atoms is remarkably stable while the local coordination of the CO_3 groups as well as the water oxygens is changing slightly.

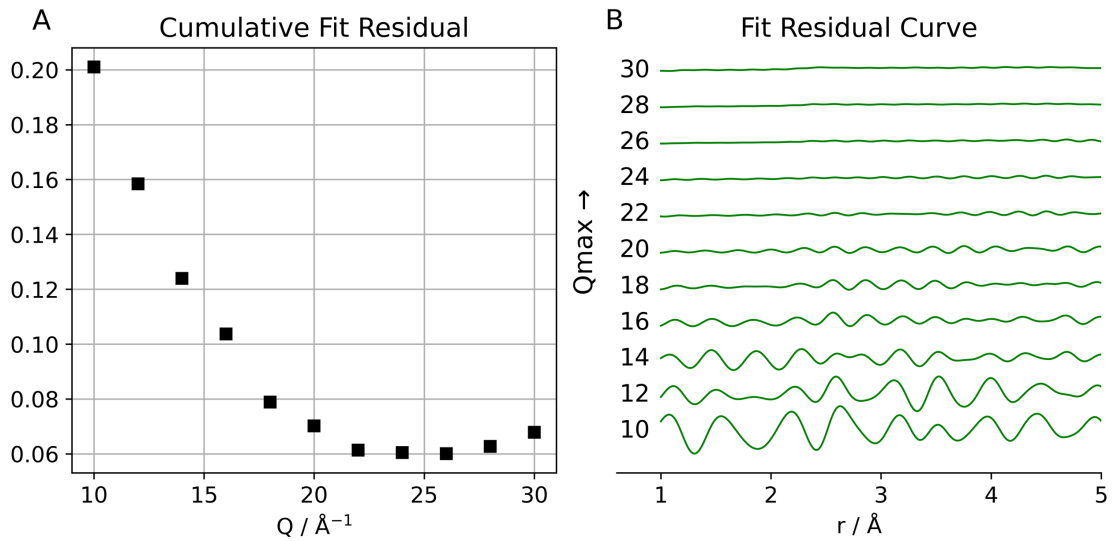

Fig. S8. Investigation on the impact on the G(r) q range on the quality of the RMC modelling. To investigate this effect, diffraction data was calculated from fully converged a fully converged RMC model and the data was truncated at various a q_{max} between 10 and 30 A^{-1}. These truncated data sets where subsequently used to refine and RMC model with just the scale factor as the only free parameter. A) L-curve showing the cumulative fit residual error as a function of the q_{max} truncation. It shows that the error drops significantly until ~20 A^{-1}, indicating that useful information is contained in this range. B) The fit residual curve shows the residual for a real-space range of 1 – 5 A for various truncations. It can be seen that severe fit residuals are present for truncations from 10 to 16 A^{-1} which progressively disappear from 18 A^{-1} onwards.

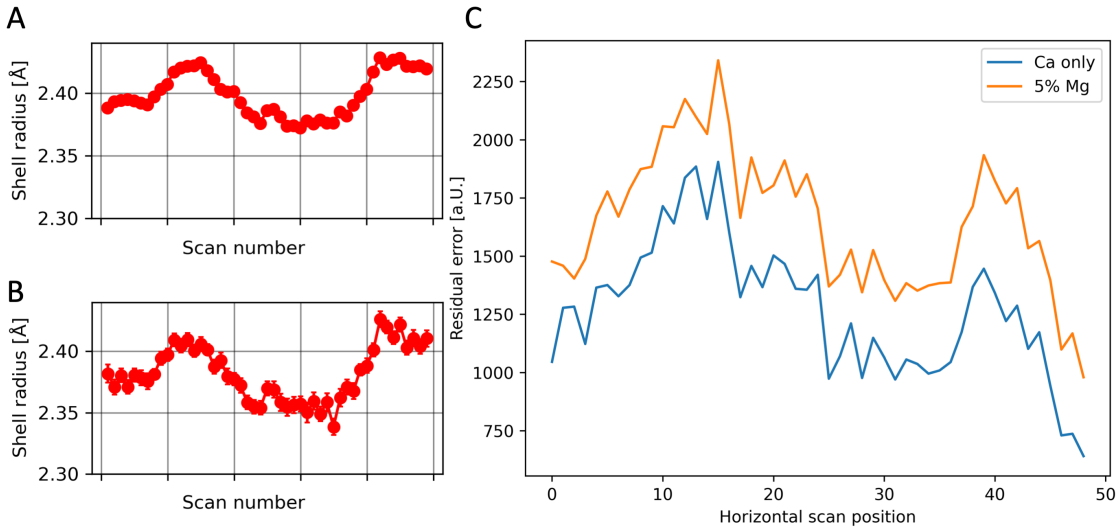

Fig. S9. Investigation of a Ca-only and a 5% Mg-substituted RMC model. In order to test the impact of Mg atoms on the RMC modelling, a RMC model with a 5% replacement of Ca atoms by Mg atoms was prepared and fitted to the horizontal line scan. Fitting restraints were adapted from the Ca atoms (see Table S1), ensuring that they leave sufficient freedom for the Mg atom pairs. (A) Ca-O atom pair distance extracted from the 5% Mg model, exhibiting a very similar behavior to the Ca-only free model shown in Fig 5. (B) Mg-O atom pair distance extracted from the 5% Mg model. The behavior is qualitatively very similar to both the Ca-O atom pair distance (A) and the Ca-O in the Mg-free model. What is observable is a slight, linear offset in the atom pair distance, most probably caused by the presence of the additional Ca-O atom pairs and the increased degrees of freedom. As the behavior of the two is rather similar, this doesn't hint towards the presence of a new compound but an artificial splitting of one existing fraction. (C) Comparison of the fit error along the horizontal line for the Ca-only and 5% Mg model. It can be seen that the 5% Mg model is consistently producing higher levels residual errors due to the larger number of variables which contribute to the error metric.

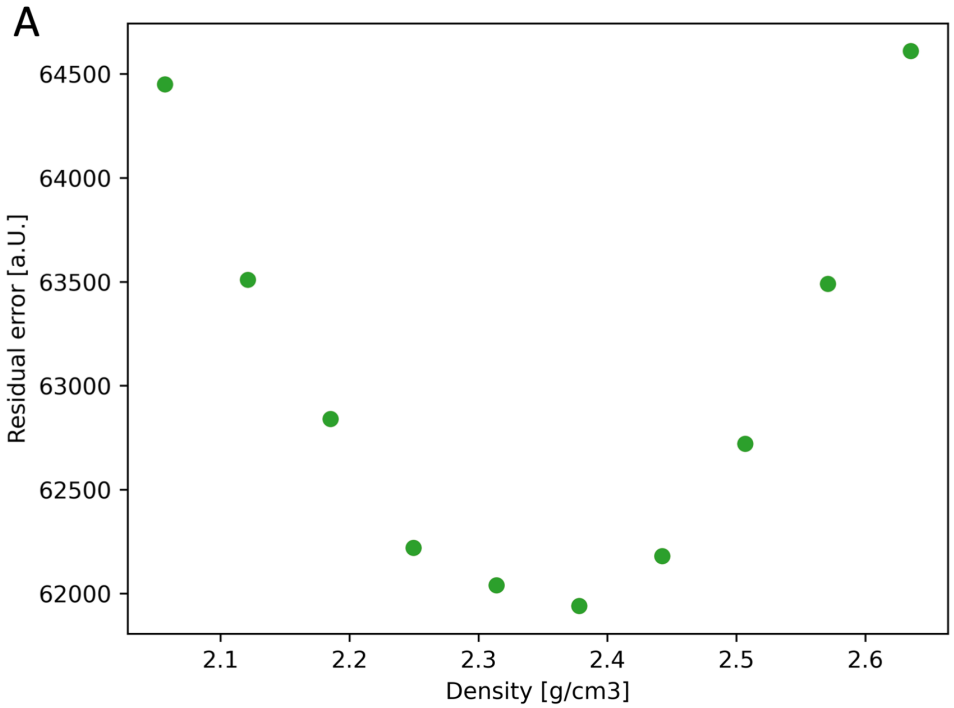

Fig. S10. Analysis of the compound density on the RMC modelling residual error. The RMC supercell density was varied in a range of 2.1 to 2.6 g/cm^3 and an RMC refinement was carried out for each density for one datapoint (horizontal #30). The residual error shows a minimum at ~2.4 g/cm^3 with a rather flat error landscape ±0.1 g/cm^3 around the minimum. The found minimum falls well within the range of reported ACC densities (1–3) and the density of 2.38 g/cm^3, which is also reported for Monohydrocalcite and was retained for the further RMC modelling.

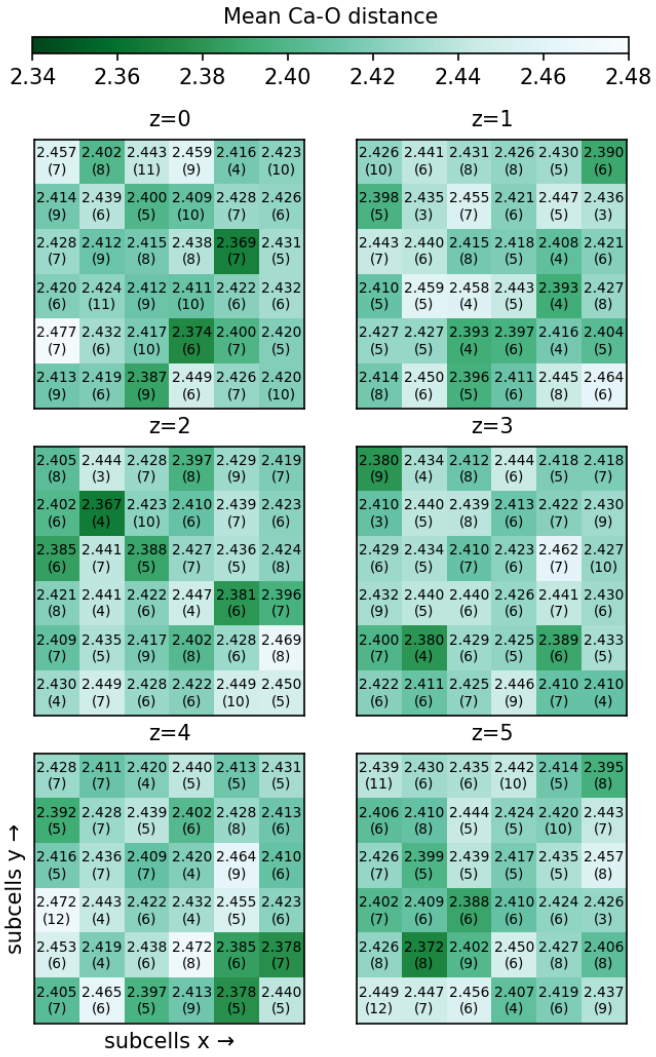

Fig. S11. Analysis of Ca-O atom pair distance distribution in the full super cell in one spot (Horizontal point #11). The 6x6x6 supercell into the individual sub-cells, each containing 9 cations. The average Ca-O atom pair distance and the standard error (in brackets) has been determined for each subcell and is presented both numerically and graphically with the color code. It is visible that the standard error in each subcell is already smaller than the overall changes in the Ca-O atom pair distance. It is also only 3-4x the standard error of the overall volume, indicating the atom pair distances are rather narrowly distributed around their mean value. The analysis also shows that while cells with shortened Ca-O atom pair distance exist but are dispersed randomly throughout the supercell volume.

Table S1. Biogenic ACC bond parameters extracted via Ca EXAFS, Mg EXAFS and PDF

			Atomic distance [A]				
Method	**Sample**	**Reference**	**Ca-O (Mg-O)**	**Ca-C**	**Ca-O (3^{rd})**	**Ca-C**	**Ca-Ca**
Ca EXAFS	Ficus retusa cystolites	Taylor 1993 (4)	2.35/2.43/2.44	2.73	3.2	-	-
	Pyura pachydermtina spicule	Levi-Kalisman 2000 (5)	2.37	-	-	3.03	3.36
	Porcellio scaber	Becker 2003(6)	2.38			3.0/3.72	3.89
	Biomphalaria glabrata egg (120h)	Hasse 2000 (7)	2.47			2.84/3.1	3.95
	Lobster carapace	Levi-Kalisman 2002 (8)	2.23/2.41			3.47	3.79
	Ficus microcarpa Cystolie		2.20/2.4			3.5	3.79
	Armadillidium vulgare	Becker 2005 (9)	2.37		3.64	3.0	4.02
	Porcellio scaber		2.37		3.64	2.99	4.05
	Homarus americanus gastrolith	Reeder 2013 (10)	2.41				
Mg EXAFS	Paracentrotus lividus P3	Politi 2006 (11)	2.3/2.48		3.59	3.35	
	Ficus microcarpa cystolith	Politi 2010 (12)	2.04				
	Homarus americanus Cuticle		2.04				
	Pyura pachydermatina		2.06				
PDF (Total PDF, no fit)	Homarus americanus gastrolith	Reeder 2013 (10)	~2.4				

Table S2. Synthetic ACC bond parameters extracted via Ca EXAFS, Mg EXAFS and PDF

			Atomic distance [A]			
Method	**Sample**	**Reference**	**Ca-O (Mg-O)**	**Ca-C**	**Ca-O (3rd)**	**Ca-Ca**
Ca EXAFS	ACC, CO2 bubbling	Becker 2005 (9)	2.41			
	ACC, precipitation	Politi 2006 (11)	2.43	3.22		
	ACC, precipitation	Michel 2008 (13)	2.41			
	Proto-Vaterite ACC	Gebauer 2010 (14)	2.39			
	Proto-Calcite ACC		2.36			
	Proto-Aragonite ACC	Farhadi-Khouzani 2016 (15)	2.41			
	ACC fresh	Schmidt 2014 (16)	2.38			
	ACC, 115°C		2.38			
	ACC 150°C		2.37			
	ACC 200°C		2.37			
13C NMR	ACC, precipitation	Singer 2012 (17)	2.45			
Partial PDF, RMC modelling	ACC precipitation, CO2 decomp	Goodwin 2010 (1)	2.47	3.5	4.1	4.0
Partial PDF, EPSR modelling	ACC, 5% Mg x 0.25 H2O	Cobourne 2013 (18)	2.41	~3.3	~4.3	~3.5

Total PDF, no fit	100% Mg-ACC	Radha 2012 (19)	2.1			
	0% Mg-ACC		2.3			
	ACC, precipitation	Michel 2008 (13)	~2.4			
	ACC x 1.4 H2O	Albéric 2018 (20)	2.38	2.92	4.05	6.20
	ACC x 0.3 H2O		2.36	2.94	4.02	6.24
	Mg-ACC x 1.4 H2O		2.4	2.90	4.1	6.24
	Mg-ACC x 0.2 H2O		2.37	2.90	4.08	6.24
	ACC fresh	Schmidt 2014 (16)	2.40			
	ACC 115°C (46% water loss)		2.38			

Table S3. Crystalline calcite bond parameters determined from X-ray diffraction

Sample	Reference	a	c	C-O	Ca-O	C-C	Ca-C
Synthetic Calcite	Zolotoyabko 2010 (21)	4.988	17.068	1.282	2.359	4.048	3.212
Geo Calcite (0% Mg corr)	Zolotoyabko 2010 (21)			1.282	2.359	4.048	3.212
Geo calcite (0.2% Mg)	Effenberger 1981 (22)	4.9896	17.061	1.281	2.360	4.048	3.212
Geo Calcite (0.2% Mg)	Markgraf and Reeder 1985 (23)	4.988	17.061	1.280	2.360	4.047	3.212
Geo Calcite (0.19% Mg)	Wang 2018 (24)	4.9828	17.0315	1.247	2.373	4.041	3.208
Calcite	Chessin 1965 (25)	4.99	17.002	1.283	2.356	4.041	3.211
Calcite	Graf 1961 (26)	4.99	17.061	1.286	2.357	4.048	3.213
Synthetic Calcite	Sitepu 2009 (27)	4.99	17.0687	1.277	2.362	4.049	3.213
Synthetic Calcite	Maslen 1995 (28)	4.988	17.068	1.286	2.357	4.048	3.213
Synthetic Calcite	Maslen 1993 (29)	4.991	17.062	1.284	2.359	4.048	3.213
Average ± Std deviation				1.279 ±0.011	2.360 ±0.005	4.047 ±0.003	3.212 ±0.002

Table S4 Comparison of scattering lengths for the atomic pairs with Ca (left column) and Mg (right column). The scattering lengths are normalized to the sum of all scattering contributions.

Scattering length of atomic pairs (normalized)	Ca	Mg
Ca	14.6	0.9
C	9.3	0.3
O	37.0	1.2
Mg	0.9	0.01

Table S5. RMC fitting bond constraints for the C, O, Ca atoms in the carbonate structure (c), water (w), and protein (p)

Type 1	Type 2	min dist [A]	max dist [A]
Cc	Cc	2.3	3.0
Cc	Cw	2.0	2.7
Cc	Oc	1.0	1.7
Cc	Ca	2.3	3.0
Cc	Cp	1	10
Cc	Op	1	10
Ow	Ow	2.3	3
Ow	Oc	2.3	3
Ow	Ca	2.0	2.7
Ow	Cp	1	10
Ow	Op	1	10
Oc	Oc	2.0	2.7
Oc	Ca	2.0	2.7
Oc	Cp	1	10
Oc	Op	1	10
Ca	Ca	2.7	3.4
Ca	Cp	1	10
Ca	Op	1	10
Cp	Cp	1.3	10
Cp	Op	1.0	1.7
Op	Op	2.0	2.7

SI References

1. A. L. Goodwin, *et al.*, Nanoporous Structure and Medium-Range Order in Synthetic Amorphous Calcium Carbonate. *Chemistry of Materials* **22**, 3197–3205 (2010).

2. M. Saharay, A. O. Yazaydin, R. J. Kirkpatrick, Dehydration-Induced Amorphous Phases of Calcium Carbonate. *J. Phys. Chem. B* **117**, 3328–3336 (2013).

3. J. Bolze, *et al.*, Formation and Growth of Amorphous Colloidal CaCO3 Precursor Particles as Detected by Time-Resolved SAXS. *Langmuir* **18**, 8364–8369 (2002).

4. M. G. Taylor, K. Simkiss, G. N. Greaves, M. Okazaki, S. Mann, An X-Ray Absorption Spectroscopy Study of the Structure and Transformation of Amorphous Calcium Carbonate from Plant Cystoliths. *Proceedings: Biological Sciences* **252**, 75–80 (1993).

5. Y. Levi-Kalisman, S. Raz, S. Weiner, L. Addadi, I. Sagi, X-Ray absorption spectroscopy studies on the structure of a biogenic "amorphous" calcium carbonate phase †. *J. Chem. Soc., Dalton Trans.*, 3977–3982 (2000).

6. A. Becker, *et al.*, Structural characterisation of X-ray amorphous calcium carbonate (ACC) in sternal deposits of the crustacea Porcellio scaber. *Dalton Trans.*, 551–555 (2003).

7. B. Hasse, H. Ehrenberg, J. C. Marxen, W. Becker, M. Epple, Calcium Carbonate Modifications in the Mineralized Shell of the Freshwater Snail Biomphalaria glabrata. *Chemistry: A European Journal* **6**, 7 (2000).

8. Y. Levi-Kalisman, S. Raz, S. Weiner, L. Addadi, I. Sagi, Structural Differences Between Biogenic Amorphous Calcium Carbonate Phases Using X-ray Absorption Spectroscopy. *Advanced Functional Materials* **12**, 6 (2002).

9. A. Becker, A. Ziegler, M. Epple, The mineral phase in the cuticles of two species of Crustacea consists of magnesium calcite, amorphous calcium carbonate, and amorphous calcium phosphate. *Dalton Trans.*, 1814 (2005).

10. R. J. Reeder, *et al.*, Characterization of Structure in Biogenic Amorphous Calcium Carbonate: Pair Distribution Function and Nuclear Magnetic Resonance Studies of Lobster Gastrolith. *Crystal Growth & Design* **13**, 1905–1914 (2013).

11. Y. Politi, *et al.*, Structural Characterization of the Transient Amorphous Calcium Carbonate Precursor Phase in Sea Urchin Embryos. *Adv. Funct. Mater.* **16**, 1289–1298 (2006).

12. Y. Politi, *et al.*, Role of Magnesium Ion in the Stabilization of Biogenic Amorphous Calcium Carbonate: A Structure−Function Investigation. *Chemistry of Materials* **22**, 161–166 (2010).

13. F. M. Michel, *et al.*, Structural Characteristics of Synthetic Amorphous Calcium Carbonate. *Chemistry of Materials* **20**, 4720–4728 (2008).

14. D. Gebauer, *et al.*, Proto-Calcite and Proto-Vaterite in Amorphous Calcium Carbonates. *Angewandte Chemie* **122**, 9073–9075 (2010).

15. M. Farhadi-Khouzani, D. M. Chevrier, P. Zhang, N. Hedin, D. Gebauer, Water as the Key to Proto-Aragonite Amorphous CaCO3. *Angew. Chem. Int. Ed.*, 5 (2016).

16. M. P. Schmidt, A. J. Ilott, B. L. Phillips, R. J. Reeder, Structural Changes upon Dehydration of Amorphous Calcium Carbonate. *Crystal Growth & Design* **14**, 938–951 (2014).

17. J. W. Singer, A. Ö. Yazaydin, R. J. Kirkpatrick, G. M. Bowers, Structure and Transformation of Amorphous Calcium Carbonate: A Solid-State ^{43} Ca NMR and Computational Molecular Dynamics Investigation. *Chemistry of Materials* **24**, 1828–1836 (2012).

18. G. Cobourne, *et al.*, Neutron and X-ray diffraction and empirical potential structure refinement modelling of magnesium stabilised amorphous calcium carbonate. *Journal of Non-Crystalline Solids* **401**, 154–158 (2014).

19. A. V. Radha, *et al.*, Energetic and structural studies of amorphous Ca1−xMgxCO3·nH2O (0⩽x⩽1). *Geochimica et Cosmochimica Acta* **90**, 83–95 (2012).

20. M. Albéric, *et al.*, The Crystallization of Amorphous Calcium Carbonate is Kinetically Governed by Ion Impurities and Water. *Adv. Sci.* **5**, 1701000 (2018).

21. E. Zolotoyabko, *et al.*, Differences between Bond Lengths in Biogenic and Geological Calcite. *Crystal Growth & Design* **10**, 8 (2010).

22. H. Effenberger, K. Mereiter, J. Zemann, Crystal structure refinements of magnesite, calcite, rhodochrosite, siderite, smithonite, and dolomite, with discussion of some aspects of stereochemistry of calcite type carbonates. *Zeitschrift für Kristallographie* **156**, 10 (1981).

23. S. A. Markgraf, R. J. Reeder, High-temperature structure refinements of calcite and magnesite. *American Mineralogist* **70**, 11 (1985).

24. M. Wang, G. Shi, J. Qin, Q. Bai, Thermal behaviour of calcite-structure carbonates: a powder X-ray diffraction study between 83 and 618 K. *ejm* **30**, 939–949 (2018).

25. H. Chessin, W. C. Hamilton, B. Post, Position and thermal parameters of oxygen atoms in calcite. *Acta Cryst* **18**, 689–693 (1965).

26. D. L. Graf, Crystallographic tables for the rhombohedral carbonates. *American Mineralogist* **46**, 1283–1316 (1961).

27. H. Sitepu, Texture and structural refinement using neutron diffraction data from molybdite (MoO_3) and calcite ($CaCO_3$) powders and a Ni-rich $Ni_{50.7}Ti_{49.30}$ alloy. *Powder Diffr.* **24**, 315–326 (2009).

28. E. N. Maslen, V. A. Streltsov, N. R. Streltsova, N. Ishizawa, Electron density and optical anisotropy in rhombohedral carbonates. III. Synchrotron X-ray studies of $CaCO_3$, $MgCO_3$ and $MnCO_3$. *Acta Crystallogr B Struct Sci* **51**, 929–939 (1995).

29. E. N. Maslen, V. A. Streltsov, N. R. Streltsova, X-ray study of the electron density in calcite, $CaCo_3$. *Acta Crystallogr B Struct Sci* **49**, 636–641 (1993).